

Journal of Biomedical Optics

SPIEDigitalLibrary.org/jbo

Two-photon excited fluorescence lifetime imaging and spectroscopy of melanins *in vitro* and *in vivo*

Tatiana B. Krasieva
Chiara Stringari
Feng Liu
Chung-Ho Sun
Yu Kong
Mihaela Balu
Frank L. Meyskens
Enrico Gratton
Bruce J. Tromberg

Two-photon excited fluorescence lifetime imaging and spectroscopy of melanins *in vitro* and *in vivo*

Tatiana B. Krasieva,^a Chiara Stringari,^b Feng Liu,^c Chung-Ho Sun,^a Yu Kong,^d Mihaela Balu,^a Frank L. Meyskens,^c Enrico Gratton,^b and Bruce J. Tromberg^a

^aUniversity of California, Beckman Laser Institute and Medical Clinic, Irvine, California 92617-1475

^bUniversity of California, Laboratory for Fluorescence Dynamics (LFD), Biomedical Engineering, Irvine, California 92697-2715

^cUniversity of California, Department of Medicine and Chao Family Comprehensive Cancer Center, Irvine, California 92697-2675

^dXi'an Jiaotong University, School of Life Science and Technology, Xi'an, Shaanxi Province, China

Abstract. Changes in the amounts of cellular eumelanin and pheomelanin have been associated with carcinogenesis. The goal of this work is to develop methods based on two-photon-excited-fluorescence (TPEF) for measuring relative concentrations of these compounds. We acquire TPEF emission spectra ($\lambda_{\text{ex}} = 1000$ nm) of melanin *in vitro* from melanoma cells, hair specimens, and *in vivo* from healthy volunteers. We find that the pheomelanin emission peaks at approximately 615 to 625 nm and eumelanin exhibits a broad maximum at 640 to 680 nm. Based on these data we define an optical melanin index (OMI) as the ratio of fluorescence intensities at 645 and 615 nm. The measured OMI for the MNT-1 melanoma cell line is 1.6 ± 0.22 while the Mc1R gene knockdown lines MNT-46 and MNT-62 show substantially greater pheomelanin production (OMI = 0.5 ± 0.05 and 0.17 ± 0.03 , respectively). The measured values are in good agreement with chemistry-based melanin extraction methods. In order to better separate melanin fluorescence from other intrinsic fluorophores, we perform fluorescence lifetime imaging microscopy of *in vitro* specimens. The relative concentrations of keratin, eumelanin, and pheomelanin components are resolved using a phasor approach for analyzing lifetime data. Our results suggest that a noninvasive TPEF index based on spectra and lifetime could potentially be used for rapid melanin ratio characterization both *in vitro* and *in vivo*. © The Authors. Published by SPIE under a Creative Commons Attribution 3.0 Unported License. Distribution or reproduction of this work in whole or in part requires full attribution of the original publication, including its DOI. [DOI: [10.1117/1.JBO.18.3.031107](https://doi.org/10.1117/1.JBO.18.3.031107)]

Keywords: two-photon-excited-fluorescence; nonlinear optical microscopy; spectroscopy; fluorescence lifetime imaging microscopy; phasor; eumelanin; pheomelanin; skin; melanoma.

Paper 12503SS received Aug. 7, 2012; revised manuscript received Oct. 2, 2012; accepted for publication Nov. 6, 2012; published online Dec. 12, 2012.

1 Introduction

Human skin and hair color are determined by melanin type and content. There are two major forms of this naturally occurring pigment: eumelanin and pheomelanin. Eumelanin is brown to black in color while pheomelanin is yellow to red. The regulation of the production of eumelanin versus pheomelanin involves the interaction of the melanocortin 1 receptor (Mc1R) on the surface of the melanocyte with melanocyte stimulating hormone (MSH) or with the agouti signaling protein. The binding of MSH to Mc1R results in the formation of eumelanin while the binding of the agouti protein to Mc1R leads to the production of pheomelanin.

Epidemiology studies have shown that red hair and light skin color are risk factors for melanoma development.^{1,2} Mutations in the human Mc1R gene are associated with red hair and light skin color, which is characterized by a high pheomelanin/eumelanin ratio.³ While eumelanin can serve as anti-oxidant to scavenge free radicals,⁴ pheomelanin can become a photosensitizer and generate reactive oxygen species after UV radiation.^{5,6}

Currently, the total melanin content in biological specimens is typically determined by measuring light absorption at 450 to 475 nm after alkaline degradation.⁷ Due to a lack of understanding of the structures of eumelanin and pheomelanin, it has not

been possible to directly measure these two types of melanins. Ito and Fujita developed an HPLC-based method to indirectly measure eumelanin and pheomelanin after a series of degradation and oxidation steps.^{8,9} Because of the complicated processing steps and amplification constant used in this method, a small error in the HPLC measurement can result in a large error in the final reading.

Rapid, nondegrading, noninvasive optical methods for melanin ratio measurements would be highly desirable. Warren et al. have developed a pump-probe imaging approach^{10,11} for separating pheomelanin from eumelanin and have demonstrated its performance in excised human pigmented lesions and *in vivo* in a murine model. Other optical approaches rely on reflectance spectroscopy¹² and absorption spectroscopy.¹³ There is a limited amount of published data on the fluorescence of naturally occurring melanins. *In vivo* excitation of fluorescence using visible light is impractical due to low quantum yields, poor light penetration in tissue, and the strong, broadband melanin absorption which can lead to self-quenching and photodamage. Near infrared (NIR) two-photon excitation is advantageous due to lower scattering, enhanced skin penetration, and reduced photodamage.

The first results for bulk melanin emission spectral properties in human skin were reported for simultaneous¹⁴ and stepwise¹⁵⁻¹⁷ two-photon excitation using 810-nm light. In this work we extend these previous studies by characterizing naturally occurring eumelanin and pheomelanin using

Address all correspondence to: Bruce J. Tromberg, University of California, Beckman Laser Institute and Medical Clinic, Irvine, California 92617-1475. Tel: (949) 824-4713; Fax: (949) 824 8413; E-mail: bjtrombe@uci.edu

two-photon excited fluorescence spectra and lifetimes. Both *in vitro* and *in vivo* measurements are obtained from melanoma cells, hair specimens, and *in vivo* from healthy volunteers. By comparing TPEF to conventional chemical separation methods, we are able to obtain new insight regarding the origin of melanin fluorescence *in vivo*. In addition, we develop a practical optical index for measuring the relative concentrations of eumelanin and pheomelanin *in vivo*.

2 Methods

2.1 Cell and Raft Cultures

MNT-1 cells are established from metastatic melanoma, which appear dark in culture. MNT-46 and MNT-62 are two clones derived from MNT-1 transfected Mc1R shRNA and selected with puromycin.

Normal human fibroblasts and normal keratinocytes were harvested from neonatal foreskin as previously described.¹⁸ Fibroblasts, MNT1, MNT46, and MNT62 were maintained in advanced DMEM supplemented with 2% Fetal Bovine Serum and 2 mM Glutmax. All routine culture medium and supplements are from Life Technology. Keratinocytes were maintained in KGM2 (Lonza). Raft cultures were prepared as previously described with slight modification. Rafts established for the current experiments have fibroblasts at a density of 100,000 cells per raft and keratinocytes at a density of 500,000 per raft. MNT cells were mixed with keratinocytes at a ratio of 1 to 10 before plating on the established dermis. At the air liquid interface, rafts were maintained in 1:1 of supplemented Advanced DMEM and KGM2 on top of a 25-mm-diameter 8-micron polycarbonate membrane (GE).

2.2 Eumelanin and Pheomelanin Measurements by HPLC

Pyrrole-2, 3, 5-tricarboxylic acid (PTCA) and 4-amino-3-hydroxyphenylalanine (4-AHP) were used as markers for eumelanin and pheomelanin content respectively and the ratio of PTCA to AHP served as the ratio of eumelanin to pheomelanin content. Eumelanin and pheomelanin samples were treated and analyzed as described by Ito and Wakamatsu^{19,20} with slight modification. In brief, eumelanin samples were oxidized with H₂O₂ under basic conditions,¹⁹ while pheomelanin structures were destroyed under reduced acidic conditions using HI and H₃PO₂.²⁰ Pheomelanin lysate was further purified via an SCX column (Hypersep SPE 500 mg/3mL SCX Hypersil column, thermo scientific, wash with 3 mL water and methanol, elute with 1 mL 5M NH₄Ac) before analysis.

Eumelanin separation was performed on a Waters e2695 system with 2478 UV detector at 269 nm using a C18 column (Atlantis T3, 4.6 × 250 mm, 5- μ m particle size). PTCA was determined in isocratic mode with a mobile phase of 18% methanol in 20-mM potassium phosphate buffer (pH 2.12) at a flow rate of 0.7 ml/min under room temperature (injection volume: 80 μ L). To determine pheomelanin, samples were analyzed with an Agilent 1100 series HPLC system consisting of, a C18 column (Atlantis T3, 4.6 × 250 mm, 5- μ m particle size), an electro-chemical detector (Agilent 35900E interface and LC-4C Amperometric Detector), a reference electrode: Ag/AgCl and a platinum working electrode. 4-AHP was eluted at a flow rate of 0.5 ml/min in gradient mode: 0 to 30 min, from 100% A to 100% B, 30 to 40 min, 100% B, equilibrate column with

100% A for 15 min before the next run. The composition of the mobile phases were A: 0.1% acetic acid in 5% methanol with 1.5-mM octanesulfonic acid sodium salt and 0.1 mM EDTA (pH 4.0); mobile phase B: 0.1% acetic acid in 90% methanol with 1.5-mM octanesulfonic acid sodium salt and 0.1 mM EDTA (pH 4.0). The working voltage was set to +700 mV.

2.3 Two-Photon Imaging and Spectroscopy

Two-photon excited fluorescence emission spectra of melanins *in vitro* were obtained using the 32-channel Meta detector of the Zeiss LSM 510 Meta NLO microscopy system. The excitation wavelength used was 900 or 1000 nm from a Chameleon-Ultra femtosecond pulsed tunable (from 690 to 1040 nm) laser (Coherent Inc.). All *in vitro* spectra were acquired at 1000-nm excitation using identical settings (excitation power, detector settings) and normalized to unity at 560 nm. All *in vivo* spectra were acquired using a 900-nm excitation wavelength. Ratios of signal intensity at 645 nm (for eumelanin) to 615 nm (pheomelanin) were measured on normalized spectra and averaged for 20–25 individual cells for each MNT-1, MNT-46, and MNT-64 cell line. Standard errors for ratios were calculated as square root of the sum of squares of standard errors calculated beforehand for each independent variable.

All *in vivo* measurements were conducted according to an approved institutional protocol, and with informed consent by all participants. Microscopy imaging and measurements of melanin spectra in human skin *in vivo* were performed on a Zeiss LSM 510 microscope equipped with an objective inverter (LSM Tech. Inc, Stewartstown, Pennsylvania). The inverter converts any inverted microscope into an upright by simultaneously changing the orientation of the objective and moving the sample off of the stage. This allows maximum flexibility in sample positioning and handling while still retaining the ability to automatically acquire *z*-stacks. An imaging dish, fixed to a post by a customized holder, provided both a way to hold the immersion medium (water) in front of an objective and an extra stabilization for the sample (skin of a human volar forearm). An arm of a volunteer was slightly pressed against the imaging dish by resting on a small platform positioned under the objective in the objective-inverter, with adjustable height. All individual spectra were normalized to unity at 560 nm. They were also corrected for a total non-melanin autofluorescence, which were similarly normalized to unity at 560 nm. Mean values as well as standard errors were calculated for each emission point (about 10 nm broad that is the best resolution determined by LSM510 hardware).

Each point represents several measurements and each measurement includes number of ROIs containing different cellular clusters.

Objectives used were Zeiss EC Plan-Neofluar (40 × N.A. = 1.3 oil immersion) for spectral measurements of melanin in hair and Zeiss Achroplan (40 × N.A. = 0.8, water immersion) for all cellular rafts and *in vivo* measurements.

2.4 Two-Photon Excited Fluorescence Lifetime Imaging Microscopy

Fluorescence lifetime images were acquired with a two-photon microscope and a Becker and Hickl 830 card (Becker and Hickl, Berlin), unless differently specified. A Ti:Sapphire laser system (Spectra-Physics Mai Tai) with 80-MHz repetition rate was used to excite the sample. The laser was coupled to a Zeiss Axiovert

S100TV microscope and controlled using scanning mirrors (Cambridge Technology Mirror scanner 6350). A Zeiss C-Apochromat ($40 \times \text{N.A.} = 1.2$, water immersion) was used in all experiments. For image acquisition the following settings were used: image size of 256×256 pixels, scan speed of $32 \mu\text{m}/\text{pixel}$. A dichroic filter (700DCSPXR, Chroma Technologies) was used to separate the fluorescence signal from the excitation laser light and the emission was further isolated by long pass 550-nm filter. The fluorescence signal was detected by a hybrid detector (HPM-100, Hamamatsu). An additional barrier filter was used to block the near IR laser source.

Frequency-domain (FD) fluorescence lifetime imaging microscopy (FLIM) data were also acquired with a similar Zeiss 710 microscope and Ti:Sapphire laser coupled to an ISS A320 FastFLIM detection module.²¹ For image acquisition the following settings were used: image size of 256×256 pixels and scan speed of $25 \mu\text{s}/\text{pixel}$. A dichroic filter (690 nm) was used to separate the fluorescence signal from the excitation laser light. For the acquisition of FD FLIM images, fluorescence was detected by a Hamamatsu H7422P-40 photomultiplier tube. A 460/80 bandpass filter was placed in front of the detector. FLIM data were collected until 100 counts in the brightest pixel of the image were acquired. Typically, the acquisition time was on the order of a few seconds. All FLIM data were acquired and processed by the SimFCS software developed at the Laboratory of fluorescence dynamics (LFD, UC Irvine).

2.5 Phasor FLIM Analysis

Every pixel of the FLIM image is transformed in one pixel in the phasor plot as previously described in Refs. 22 and 23. When fluorescence lifetime data are acquired in the time domain, the components g (x -coordinate) and s (y -coordinate) of the phasor plot are given by the following expressions:

$$g_{i,j}(\omega) = \frac{\int_0^\infty I_{i,j}(t) \cos(\omega t) dt}{\int_0^\infty I_{i,j}(t) dt}, \quad (1)$$

$$s_{i,j}(\omega) = \frac{\int_0^\infty I_{i,j}(t) \sin(\omega t) dt}{\int_0^\infty I_{i,j}(t) dt}, \quad (2)$$

where the indices i and j identify a pixel of the image and ω frequency ($\omega = 2\pi f$), f is the laser repetition rate (i.e., 80 MHz in our experiment). All phasor plots are calculated at 80 MHz (i.e., the first harmonic of the laser repetition rate).

In the case of a single exponential decay $\tau = Ae^{-t/\tau}$ the coordinates are given by:

$$g(\omega) = \frac{1}{1 + (\omega\tau)^2}, \quad (3)$$

$$s(\omega) = \frac{\omega\tau}{1 + (\omega\tau)^2}, \quad (4)$$

where τ is the lifetime of the decay and ω is the laser frequency. There is a direct relationship between a phasor location and lifetime. Every possible lifetime can be mapped into this universal representation of the decay (phasor plot). All possible single exponential lifetimes lie on the “universal circle” defined as the semicircle going from point (0, 0) to point (1, 0) with radius 1/2. Point (1, 0) corresponds to $\tau = 0$, while point (0, 0) to τ .

In the phasor coordinates the single lifetime components add directly because the phasor follows the vector algebra. A mixture of two distinct single lifetime components, each of which lie separately on the single lifetime semicircle, does not lie on the semicircle. All the combination of two single exponential components must be along the line joining the two lifetime points. In a system with many single lifetime components the phasor coordinate g and s are described as:

$$g(\omega) = \sum_k \frac{h_k}{1 + (\omega\tau_k)^2}, \quad (5)$$

$$s(\omega) = \sum_k \frac{h_k \omega \tau_k}{1 + (\omega\tau_k)^2}, \quad (6)$$

where k is the intensity weighted fractional contribution of the single-exponential component with lifetime τ_k . The phasor location of the mixture of single-lifetimes is the intensity-weighted average of the contributions of each single-lifetime that lie separately on the semicircle.

In general in a system with multiple fluorescent components such as tissue, the overall decay is a phasor that is the sum of the independent phasors of each fluorescence component:

$$G(\omega) = \sum_n f_n g_n(\omega), \quad (7)$$

$$S(\omega) = \sum_n f_n s_n(\omega), \quad (8)$$

where f_n is the fractional contribution of each component characterized by the phasor coordinates g_n and s_n . Two molecular species with multi-exponential decay are identified by two specific points in the phasor plot inside the semicircle. All possible weighting of the two molecular species form phasors distributed along a straight line joining the “pure” phasors of the two species. In the case of three molecular species, all the possible combinations are contained in a triangle where the vertices correspond to the phasor of the pure species. The phasor plot of an N -component mixture will be contained in a polygon with N -vertices located in the position of the phasor of each contributing component.

The analysis of the phasor distribution was performed by cluster identification. Clusters of pixel values were detected in specific regions of the phasor plot. The calculation of the fractional intensities f_n of different fluorescence components that contribute to the signal is performed by a linear estimation on the system in each pixel described by Eqs. (7) and (8) by graphically resolving the sum of phasors. All phasor transformation and the data analysis of FLIM data are performed using SimFCS software developed at the laboratory of fluorescence dynamics (LFD, UC Irvine).

3 Results

3.1 TPEF Spectroscopy Approach

We used human hair of different colors (red, black, and gray) as a source of naturally occurring eumelanin, pheomelanin, and keratin. Melanins are produced by melanocytes located in the hair follicles in skin (dermis) and deposited in melanosomes, which then distribute along the hair shaft during the hair growth

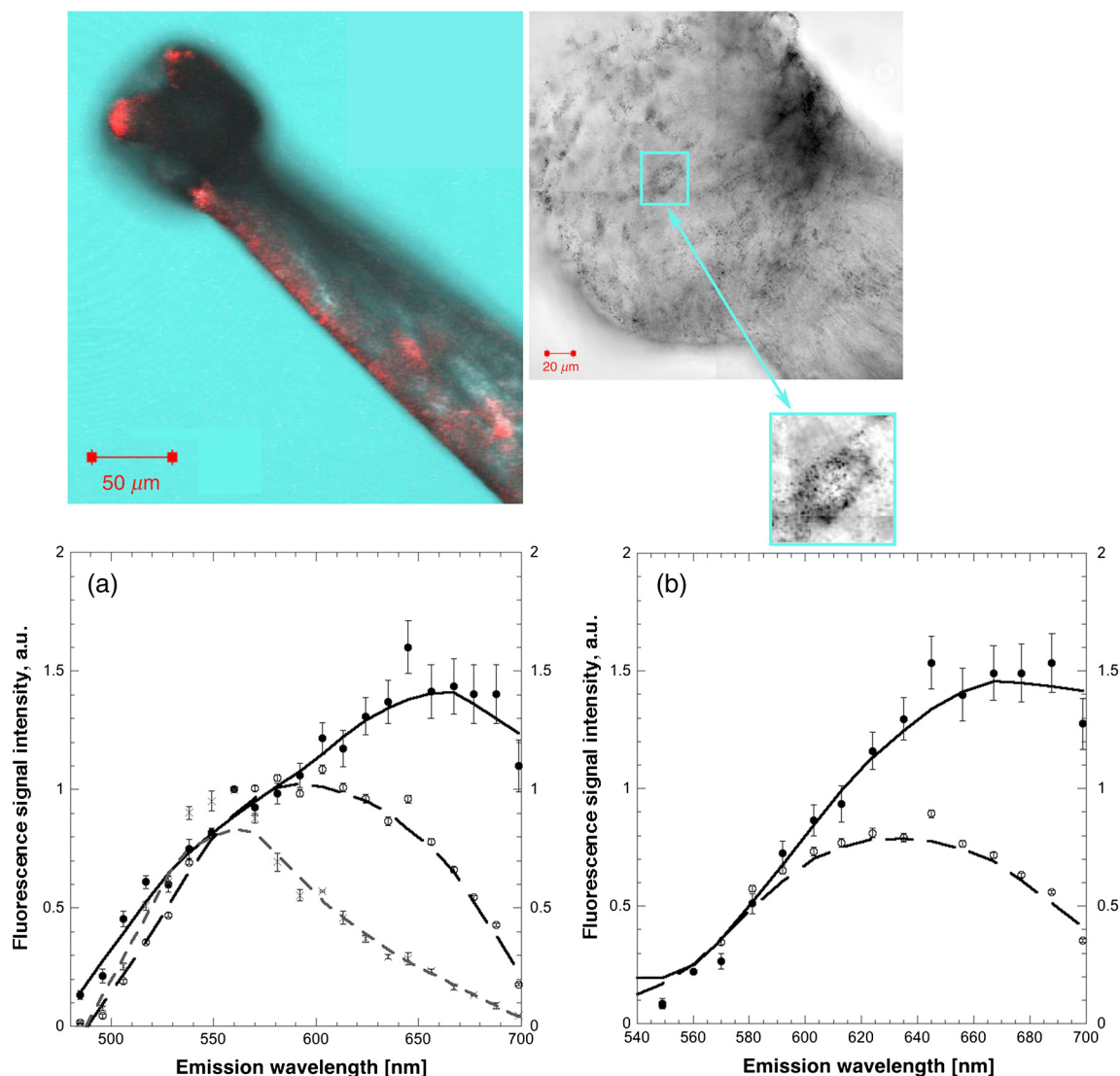


Fig. 1 Light brown human hair. Images: (lower magnification) overlay of TPEF (red, excitation 1000 nm, emission 600 to 700 nm,) on conventional light transmitted bright field mode (cyan); higher magnification—bright field images showing melanosomes. Graphs: (a) fluorescence emission spectra of red (open circle), black (filled circle) and gray (squares) human hair; excitation wavelength is 1000 nm; (b) fluorescence emission spectra of pheomelanin (circles, red hair) and eumelanin (squares, black hair) after autofluorescence (gray hair) subtraction.

(Fig. 1). The pigment in blond and red hair contains predominantly pheomelanin, while dark brown and black color is due to prevalence of eumelanin. Gray hair is devoid of any pigment.²⁴

Fluorescence was excited at 1000 nm and the resulting emission spectra were recorded and normalized to unity at 560 nm [Fig. 1(a)]. The spectrum of a colorless gray hair represented a sum of all of native cellular and extracellular (mainly keratin) fluorescence signals not associated with melanin, and it was subtracted from the spectra of pigmented samples. The remaining portion was attributed to fluorescence emission of eumelanin (black hair) and pheomelanin (red hair) [Fig. 1(b)].

Pheomelanin fluorescence emission peaked around 615 to 625 nm. Eumelanin displayed red-shifted (compared to pheomelanin) broad fluorescence emission at 640 to 680 nm and possibly was limited by the detection range of our photomultiplier tube and optical setup (up to 700 nm). Samples that mainly contained red pigment didn't show any signs of damage after scanning with both 900 nm and 1000 nm. Samples with significant

content of eumelanin (all dark brown and black samples) showed a very high susceptibility to photodamage (burns) by a scanning laser at a much lower incident power. This is most probably due to one-photon absorption of NIR light by eumelanin. Excitation at 1000 nm was deemed more appropriate due to less absorbance and hence less damage to dark samples, while peak emission intensity was comparable to that obtained at 900 nm. Excitation wavelengths longer than 1000 nm weren't practical because of a sharp drop in the laser output power and light transmission properties of the microscope objectives.

In order to ascertain the utility of spectral measurements toward the development of an optical melanin index (OMI), we searched for relevant biological samples with different melanin ratios that could be characterized by some alternative and established methods. We used a set of three human melanoma-derived cell lines (MNT-1, MNT-46, and MNT-62). MNT-1 cells originate from human metastatic melanoma. MNT-46 and MNT-62 are two Mc1R gene knockdown clones derived from MNT-1. Both clones showed about 70 to 80% of reduced protein

accumulation of Mc1R as examined by western blot (data not shown) and suggest a drastic change in eumelanin/pheomelanin ratio.^{25,26} The ratios of eumelanin to pheomelanin were measured by a novel high-performance liquid chromatography method described above. We defined the OMI as a ratio of fluorescence signal intensities measured at 645 nm (eumelanin) and 615 nm (pheomelanin), and compared the experimental results obtained by chemical (HPLC) and optical methods.

For optical measurements, MNT cells were co-cultured with human keratinocytes and seeded in 3-D collagen scaffolds to maintain melanin production. The rafts were transferred to 35-mm imaging Petri dishes with coverslips #1 on the bottom immediately before the imaging. Rafts were “flipped” to place cells directly onto the coverslip. The spectra were obtained from 20 to 30 pigmented cells for each cell line. Spectra were corrected by subtracting the autofluorescence from naturally non-pigmented melanoma cells present in each sample. Autofluorescence spectra were also averaged and normalized to unity at 560 nm as the spectra from the pigmented cell. Figure 2

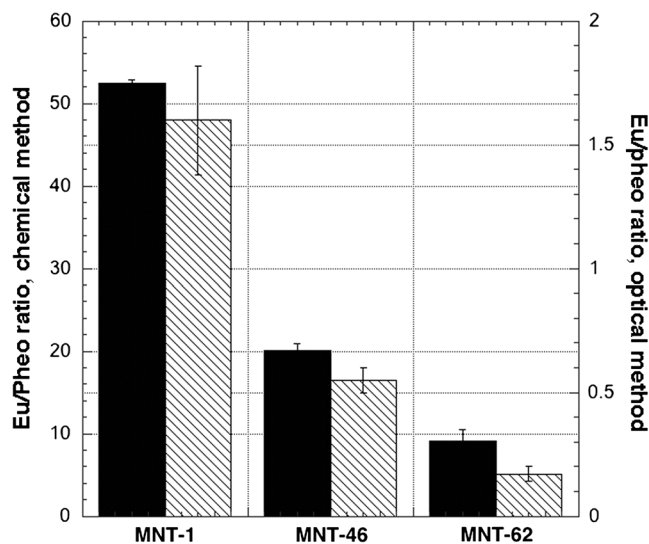


Fig. 2 Comparison of ratios of eumelanin to pheomelanin measured with HPLC-based chemical (solid bar, left axis) and optical fluorescence emission analysis (hashed bar, right axis).

shows a good correlation between the eumelanin/pheomelanin ratios measured by HPLC and the fluorescence emission analysis. Because quantum yields of fluorescence are unknown for both pigments, the numeric values for ratios obtained by chemical and optical methods are different.

To test if we could detect “fluorescence signatures” of the two melanins and measure their ratios *in vivo*, we performed microscopy imaging and measurements of melanin spectra on volar forearm skin of five healthy human subjects with different skin types (I, II-III, V, and VI).

Images (Fig. 3) and spectra (Fig. 4) were acquired at the epidermal-dermal junction and in epidermis below the stratum corneum (data not shown). Epidermal-dermal junction provided the most reliable data because the basal cellular layer containing pigmented cells (both melanocytes and keratinocytes) was easily discernible as surrounding dermal papilla.²⁷ Papilla contain fibrillar collagen producing strong second harmonic generation (SHG) signal, which makes the identification easy (Fig. 3).

OMI were calculated for normal human skin *in vivo* by the same procedure as was used for cells *in vitro*, including a normalization to unity at 560 nm and correction of normalized spectra by subtraction of autofluorescence of non-pigmented cells measured in upper epithelial layers. Average OMI for basal cells layers (melanocytes and keratinocytes) measured in skin type I, II-III (not tanned and lightly tanned) were 0.5 ± 0.1 , 1.05 ± 0.2 , and 1.16 ± 0.1 , respectively.

We could not reach the epidermal-dermal junction in the highly pigmented skin type V-VI or dependably detect the presence of pheomelanin in more superficial layers of epidermis in the darkly pigmented (primarily by eumelanin) skin types. This reduced depth of penetration may be partially attributed to more efficient absorption by melanin and scattering by melanosomes of both the excitation and emission light in upper layers of the epidermis.

This difficulty should not discourage the development of optical methods for characterizing pigmentation of normal skin and pigmented lesions. Lighter skin is a major risk factor for developing UV-induced skin diseases. Thus, for type I/II skin, TPEF spectroscopy offers a noninvasive, relatively rapid method of imaging and measurement of two forms of naturally occurring melanins as two distinct components. Nevertheless,

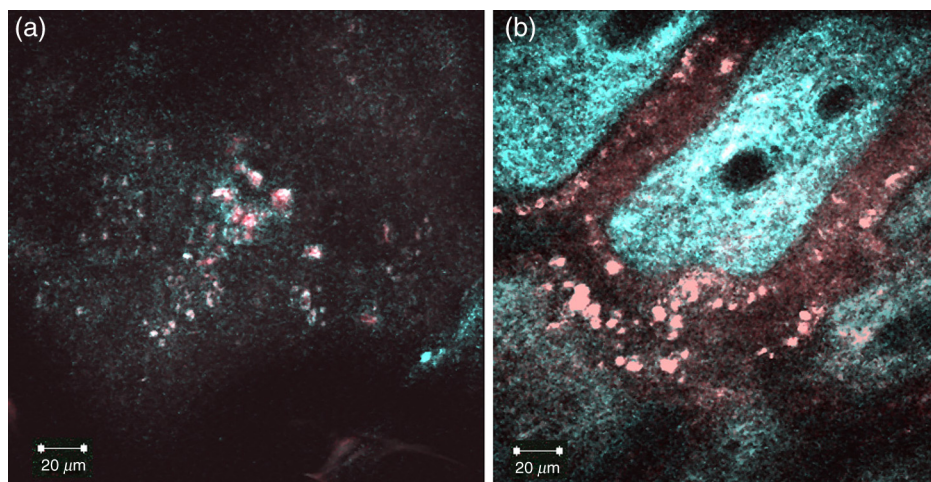


Fig. 3 *En face* images of epidermal-dermal junction at the depths of 45 μm (a) and 60 μm (b) (human skin *in vivo*). Blue: SHG of collagen; red: melanin fluorescence in melanocytes and keratinocytes, white-NIR confocal reflectance. Ex = 900 nm.

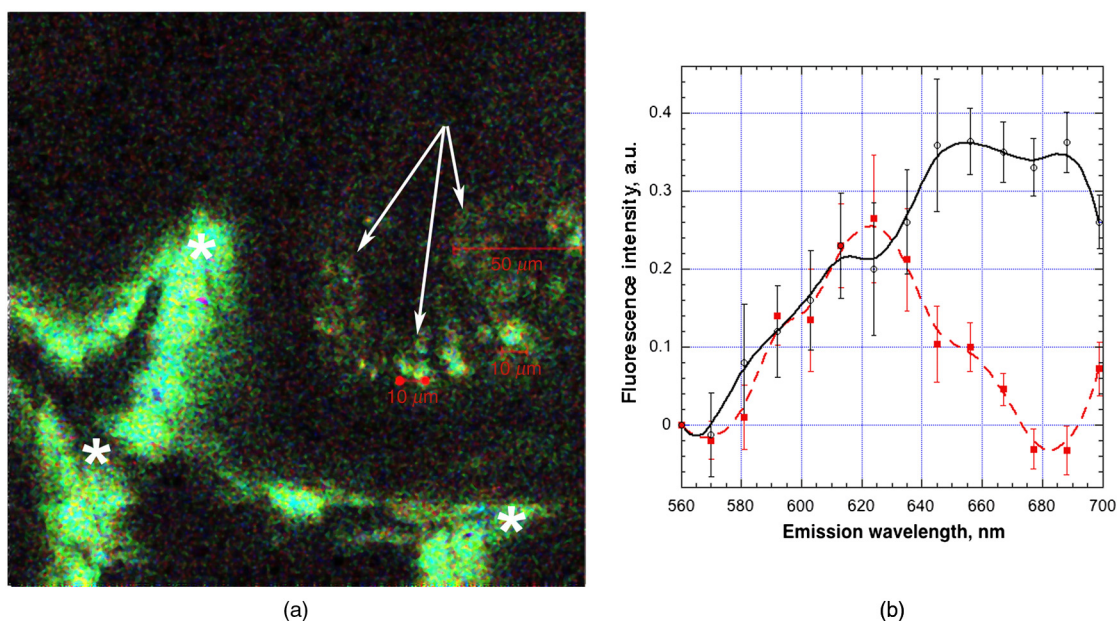


Fig. 4 (a) Hyperspectral image of epidermal-dermal junction of skin type II/III. (b) Corrected TPEF emission spectra of melanins in skin type I (broken line, red) and tanned skin type II/III (solid line, black) acquired *in vivo*. Spectra were collected on the areas of image covered by cells (both melanocytes and keratinocytes, arrows) and corrected as described in the text. Diffuse green-yellow fluorescence (white asterisks, spectrum not shown) is from keratin of stratum corneum. Excitation wavelength is 900 nm. Depth of acquisition is 45 to 55 μm . Bars represent standard error calculated for several measurements of the same subject.

a complex mixture of fluorophores that coexist and co-emit in pigmented cells makes individual components in a raw spectrum impossible to resolve. This challenge leads to a need for additional assumptions and processing. Processing involves subtraction of a residual contribution to the spectra of other fluorophores present in cells, such as flavoproteins and keratin, which can present a challenge and be a source of inaccuracy in measurements.

3.2 Phasor FLIM Approach

In addition to spectra, fluorescence can also be characterized by lifetime. Fluorescence lifetime measurements are independent of fluorophore concentration, so fluorescence lifetime imaging (FLIM) avoids some of the uncertainties and artifacts of fluorescence intensity-based measurements. Another major advantage of the FLIM approach is a distinct separation between different intracellular and extracellular fluorescence signals, thus making independent measurements and correction for all “non-pigment associated” signals unnecessary, unlike the case of spectral imaging and quantification. Moreover, the use of phasor FLIM reports not only the spatial localization of different components but also their relative concentration if they are measured simultaneously. Their measured position on the phasor diagram would be indicative of their comparative concentration [see methods, Eqs. (5) to (8)].^{22,23}

As in our spectral fluorescence measurements, black, red, and gray human hairs were used as a major source of eumelanin, pheomelanin, and keratin, respectively, to create a “FLIM fingerprint” database (Fig. 5). Non-pigmented keratin and the two different types of melanin can be easily identified and separated by their specific location in the phasor plot regardless of their complex multi-exponential lifetime decay [Fig. 5(a)]. The broad lifetime distribution measured in black and red hair [Fig. 5(d) and 5(e)] has a characteristic linear-elongated pattern that

reflects a mixture of keratin-eumelanin and of keratin-pheomelanin, respectively, possibly yielding information on different levels of melanin oligomerization.

Maps of relative concentration of keratin and the two different types of melanin highlight the round melanosomes (indicated by black arrows) that are aligned along the shaft of a black [Fig. 5(b)] and a red hair [Fig. 5(c)]. Phasor FLIM signatures of melanins in skin cells [Fig. 6(a)] (human melanocytes from skin type II, both melanins should be present) show a good correlation with the melanins measured in hair samples, which we are using as our calibration standard. Morphological features also support the attribution of those specific FLIM signatures to melanins. Intensity and FLIM patterns of melanin fluorescence [Fig. 6(c) and 6(e)] do not follow those of NADH [Fig. 6(d) and 6(f)], one of the strongest natural intracellular multiphoton excited fluorophores [Fig. 6(e) to 6(g)].

These round melanosomes [Fig. 6(c) to 6(e)] indicated by white arrows are also clearly visible in the cytoplasm of the melanoma MNT cell lines [Fig. 7(a) to 7(c)] previously used to quantify of the eumelanin-to-pheomelanin ratio as described above.

Phasor FLIM signatures of the malignant melanoma cell lines MNT-1, MNT-46, and MNT-62 cells are strikingly different [Fig. 7(d) to 7(f)] and provide a straightforward measurement of eumelanin and pheomelanin relative concentrations [Fig. 7(h) to 7(i)]. By using the phasor FLIM fingerprint of melanins obtained in Fig. 5, we directly measure [Fig. 7(h) to 7(i)] and visualize [Fig. 7(a) to 7(c)] the relative concentrations of eumelanin and pheomelanin in the different types of melanoma cells. MNT-1 are characterized by a high concentration of eumelanin with respect to pheomelanin, while MNT-46 and MNT-62 contain progressively lower concentrations of eumelanin [Fig. 7(g)–7(i)]. These results are in agreement with the ratios of eumelanin to pheomelanin measured with HPLC and optical fluorescence emission analysis in Fig. 2.

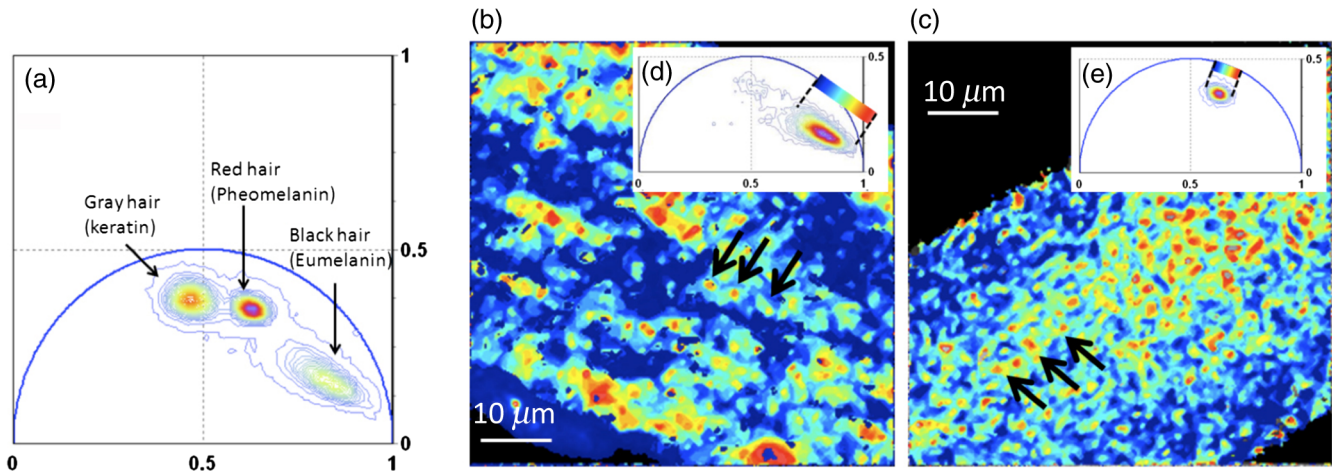


Fig. 5 (a) Phasor plot of black hair (containing predominantly eumelanin), red hair (containing predominantly pheomelanin), and gray hair (containing predominantly keratin). Excitation wavelength 900 nm, emission was isolated with long-pass (lp 550 nm) filter. The color scale (from blue to purple) corresponds with the 64 levels of the contours that indicate the percent occurrence in the phasor histogram of the pixels of the image; (b) and (c): FLIM color map of black hair (b) and red hair (c) showing the relative concentration of melanins and keratin, according to the linear cluster of (d) and (e), respectively; (d) and (e): phasor plot selection using linear cluster combination representing all possible relative contributions of keratin (blue) and eumelanin (red-yellow) for black hair (d) and relative contributions of keratin (blue) and pheomelanin (red-yellow) for red hair (e); each point along the line has a color that corresponds with a specific relative concentration of the two chemical species. Melanosomes are indicated by the black arrows.

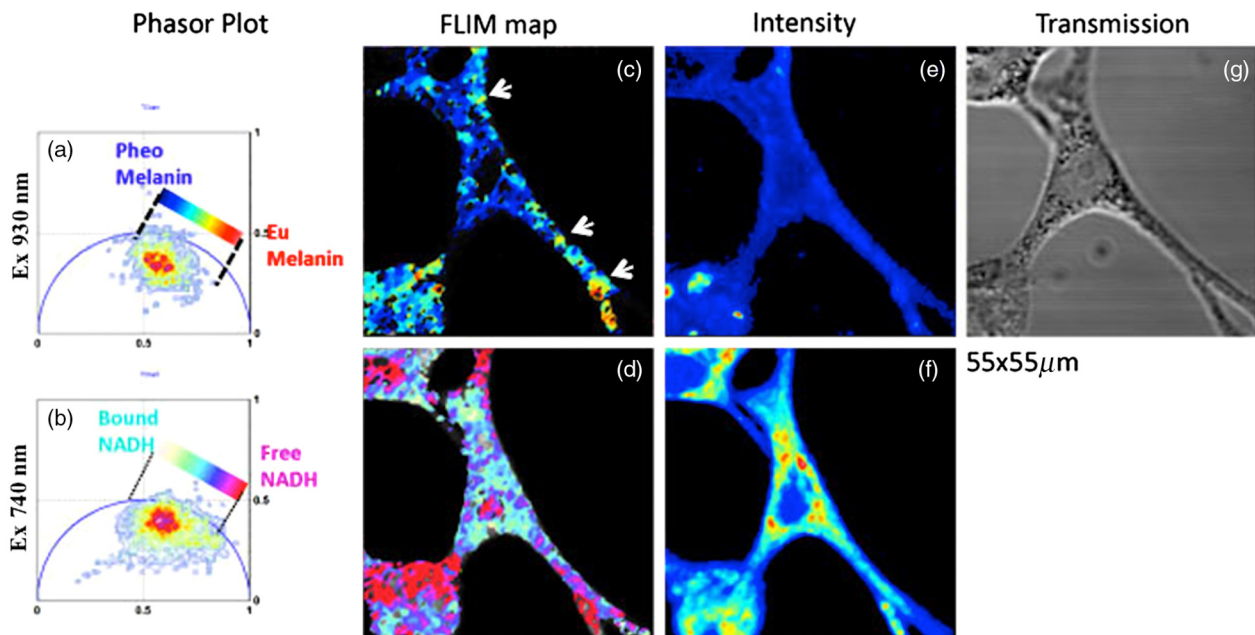


Fig. 6 Melanin and NADH distribution within abnormal melanocyte derived from skin type II. (a) FLIM phasor plot of melanin autofluorescence. Excitation wavelength 930 nm, emission is isolated with long-pass (lp 545 nm) filter. Phasor plot selection using linear cluster combination that represents all the possible relative contributions of pheomelanin (blue) and eumelanin (red-yellow). Each point along the line has a color that corresponds with a specific relative concentration of the two chemical species. (b) FLIM phasor plot of NADH autofluorescence. Excitation wavelength 740 nm, emission is isolated with bandpass (bp 545 nm) filter. Phasor plot selection using linear cluster combination that represents all the possible relative concentrations of bound NADH and free NADH. The phasor locations of pure bound and free NADH have been measured in Eq. (1)–(8). Each point along the line has a color corresponding with specific relative concentration of bound/free NADH; (c) phasor color map images representing the relative concentrations of pheomelanin (blue) and eumelanin (red-yellow). Melanosomes are indicated by the white arrows; (d) phasor color map images representing the relative concentrations of bound (cyan) and free (purple) NADH. (e) to (g): Two-photon fluorescence intensity image of a normal melanocyte excited at wavelength 930 nm (e) and 740 nm (f), and transmission image (g).

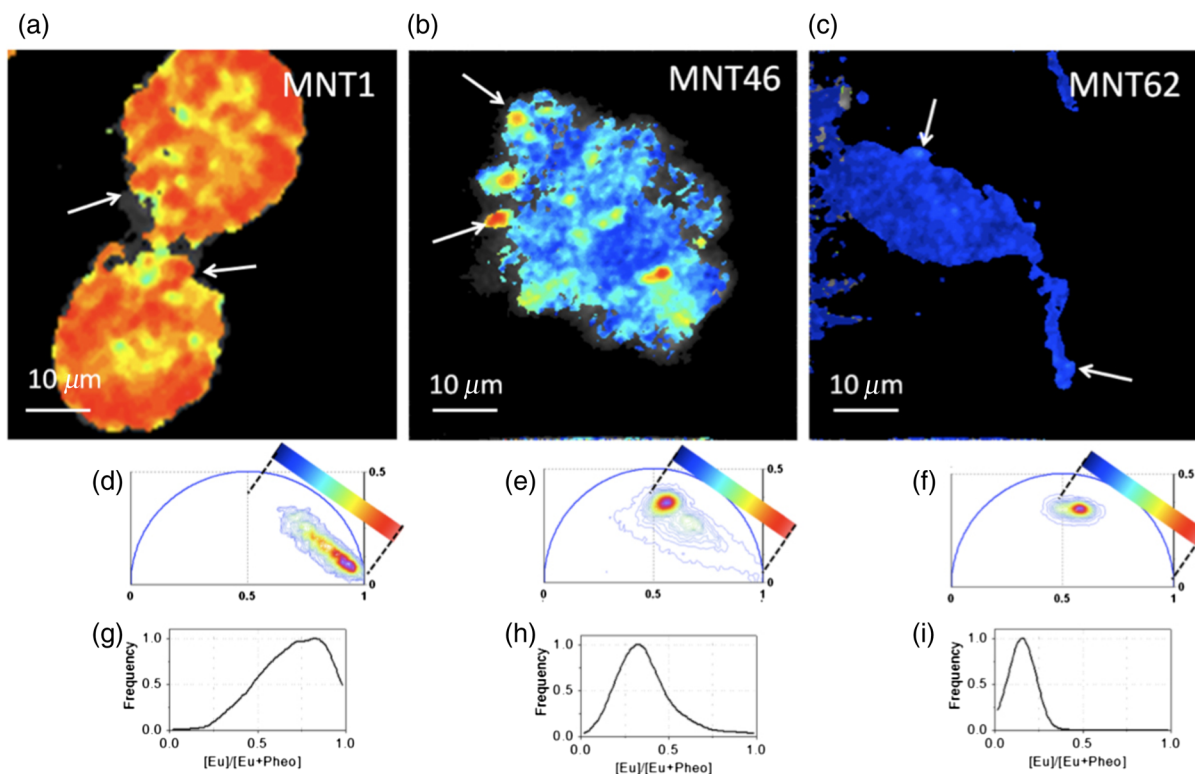


Fig. 7 (a) and (c): FLIM color maps of MNT-1 (a), MNT-46 (b), and MNT-62 (c) cells representing the relative concentration of pheomelanin and eumelanin according to the linear cluster of Figs. (d) and (f). Melanosomes are indicated by the white arrows. (d) to (f) Phasor lifetime distribution of MNT-1 (d), MNT-46 (e), and MNT-62 (f). Every phasor plot represents the lifetime distribution of 20 to 30 cells. Phasor plot selection using linear cluster combination that represents all the possible relative contributions of pheomelanin (blue) and eumelanin (red-yellow). Each point along the line has a color that corresponds with a specific relative concentration of the two chemical species. (g) to (i) Histograms of the relative concentration of Eumelanin with respect to Pheomelanin: ($[Eu]/[Eu + Pheo]$ fraction) in MNT1 (a), MNT46 (b), and MNT62 (c), cells of Figs. (a) to (c).

4 Conclusions

We have measured two-photon excited fluorescence emission spectra and lifetimes of two forms of melanin, eumelanin, and pheomelanin, naturally occurring in human skin. In order to ascertain the utility of noninvasive microscopy-based measurements in the development of an OMI, we evaluated these signatures in three human melanoma-derived cell lines. The optically derived ratios of eumelanin to pheomelanin were compared with chemical extraction and separation methods using HPLC. Spectral OMI values correlated well with HPLC-derived data over a range of cell types. Spectral measurements of light human skin types (I to III) *in vivo* showed expected increases in measured OMI values with Type I exhibiting the lowest OMI. Two-photon excited fluorescence lifetime imaging and the phasor approach to FLIM were used to overcome difficulties associated with the inability of the spectral approach to correct for autofluorescence of non-pigmented cellular and tissue compounds. Phasor FLIM provided a clear fingerprint identification of keratin, eumelanin, and pheomelanin and straightforward quantitation of relative concentration. Although the microscopy system used for FLIM measurements was not equipped for *in vivo* studies, such measurements are possible with further technical development. These data suggest that a noninvasive TPEF spectral index and phasor FLIM could potentially be used for rapid melanin ratio characterization both *in vitro* and *in vivo*.

Acknowledgments

This work was supported by the National Institutes of Health Grants P41RR01192 and P41EB015890 (Laser Microbeam and Medical Program), NCI-2P30CA62203 (University of California, Irvine Cancer Center Support Grant). CS and EG acknowledge support by the National Center for Research Resources (NCRR, 5P41RR003155) and the National Institute of General Medical Sciences (NIGMS, 8P41GM103540) divisions of the National Institutes of Health (NIH) and 5P50 GM076516. Beckman Laser Institute programmatic support from the Arnold and Mabel Beckman Foundation and is gratefully acknowledged.

References

1. D. F. Gudbjartsson et al., "ASIP and TYR pigmentation variants associate with cutaneous melanoma and basal cell carcinoma," *Nat. Genet.* **40**(7), 886–891 (2008).
2. R. A. Sturm, "Skin colour and skin cancer -MC1R, the genetic link," *Melanoma Res.* **12**(5), 405–416 (2002).
3. L. Naysmith et al., "Quantitative measures of the effect of the melanocortin 1 receptor on human pigmentation status 1," *J. Investig. Dermatol.* **122**(2), 423–428 (2004).
4. T. Sarna et al., "Interaction of radicals from water radiolysis with melanin," *Biochim. Biophys. Acta (BBA)—General Subjects* **883**(1), 162–167 (1986).
5. H. Z. Hill and G. J. Hill, "UVA, pheomelanin and the carcinogenesis of melanoma," *Pigment Cell Res.* **13**(Suppl 8), 140–144 (2000).

6. K. Jimbow, "Current update and trends in melanin pigmentation and melanin biology," *Keio J. Med.* **44**(1), 9–18 (1995).
7. A. L. Kadakaro et al., "Cutaneous photobiology. The melanocyte vs. the sun: who will win the final round?" *Pigment Cell Res.* **16**(5), 434–447 (2003).
8. S. Ito and K. Wakamatsu, "An improved modification of permanganate oxidation of eumelanin that gives a constant yield of pyrrole-2,3,5-tricarboxylic acid," *Pigment Cell Res.* **7**(3), 141–144 (1994).
9. S. Ito and K. Fujita, "Microanalysis of eumelanin and pheomelanin in hair and melanomas by chemical degradation and liquid chromatograph," *Anal. Biochem.* **144**(2), 527–536 (1985).
10. T. E. Matthews et al., "In vivo and ex vivo epi-mode pump-probe imaging of melanin and microvasculature," *Biomed. Opt. Express* **2**(6), 1576–1583 (2011).
11. T. E. Matthews et al., "Pump-probe imaging differentiates melanoma from melanocytic nevi," *Sci. Translat. Med.* **3**(71), 71ra15 (2011).
12. R. Marchesini, A. Bono, and M. Carrara, "In vivo characterization of melanin in melanocytic lesions: spectroscopic study on 1671 pigmented skin lesions," *J. Biomed. Opt.* **14**(1), 014027 (2009).
13. G. Zonios et al., "Melanin absorption spectroscopy: new method for noninvasive skin investigation and melanoma detection," *J. Biomed. Opt.* **13**(1), 014017(2008).
14. K. Hoffmann et al., "Selective femtosecond pulse-excitation of melanin fluorescence in tissue," *J. Investigat. Dermatol.* **116**(4), 629–630 (2001).
15. D. Leupold et al., "The stepwise two-photon excited melanin fluorescence is a unique diagnostic tool for the detection of malignant transformation in melanocytes," *Pigment Cell Melanoma Res.* **24**(3), 438–445 (2011).
16. M. Scholz et al., "Uncovering of melanin fluorescence in human skin tissue," *Proc. SPIE* **6633**, 663321 (2007).
17. K. Teuchner et al., "Fluorescence studies of melanin by stepwise two-photon femtosecond laser excitation," *J. Fluoresc.* **10**(3), 275–281 (2000).
18. L. L. Chiu et al., "Photodynamic therapy on keloid fibroblasts in tissue-engineered keratinocyte-fibroblast co-culture," *Lasers Surg. Med.* **37**(3), 231–244 (2005).
19. S. Ito and K. Wakamatsu, "Chemical degradation of melanins: application to identification of dopamine-melanin," *Pigment Cell Res.* **11**(2), 120–126 (1998).
20. K. Wakamatsu and S. Ito, "Advanced chemical methods in melanin determination," *Pigment Cell Res.* **15**(3), 174–183 (2002).
21. R. A. Colyer, C. Lee, and E. Gratton, "A novel fluorescence lifetime imaging system that optimizes photon efficiency," *Microsc. Res. Techniq.* **71**(3), 201–213 (2008).
22. C. Stringari et al., "Phasor approach to fluorescence lifetime microscopy distinguishes different metabolic states of germ cells in a live tissue," *Proc. Natl. Acad. Sci.* **108**(33), 13582–13587 (2011).
23. M. A. Digman et al., "The phasor approach to fluorescence lifetime imaging analysis," *Biophys. J.* **94**(2), 14–16 (2008).
24. R. M. Haywood, M. Lee, and C. Andraday, "Comparable photoreactivity of hair melanosomes, eu- and pheomelanins at low concentrations: low melanin a risk factor for UVA damage and melanoma?" *Photochem. Photobiol.* **84**(3), 572–581 (2008).
25. Z. A. Abdel-Malek et al., "The melanocortin 1 receptor and the UV response of human melanocytes—a shift in paradigm," *Photochem. Photobiol.* **84**(2), 501–508 (2008).
26. M. C. Scott et al., "Human melanocortin 1 receptor variants, receptor function and melanocyte response to UV radiation," *J. Cell Sci.* **115**(11), 2349–2355 (2002).
27. E. Dimitrow et al., "Sensitivity and specificity of multiphoton laser tomography for in vivo and ex vivo diagnosis of malignant melanoma," *J. Invest. Dermatol.* **129**(7), 1752–1758 (2009).